Assessment of Short-medium Term Intervention Effects Using CAESAR-Lisflood in Post-earthquake Mountainous Area

Di Wang[1,2,3], Ming Wang[1], Kai Liu[1]

[1]School of National Safety and Emergency Management, Beijing Normal University, Beijing, China.

[2]Academy of Disaster Reduction and Emergency Management, Beijing Normal University, Beijing, China.

[3]Faculty of Geographical Science, Beijing Normal University, Beijing, China.

Correspondence to: Ming Wang (wangming@bnu.edu.cn)

Abstract. The 2008 Wenchuan earthquake triggered local geomorphic changes rapidly and gradually, producing abundant materials through external processes. The substantial materials increased the risks of geomorphic hazards (flash floods, landslides, and debris flows) induced by extreme precipitation in the area. Intervention measures such as dams, levees, and vegetation revetments have been constructed in specified sites to reduce sediment transport.

This study concentrated on assessing intervention effects incorporated with various facilities on post-earthquake fragile mountains in the short-medium term. Taking the Xingping valley as an example, we used the CAESAR-Lisflood landscape evolution model to simulate three scenarios: unprotected landscapes, present protected landscapes, and enhanced protected landscapes between 2011 and 2013. We compared the geomorphic changes and defined two indicators to assess the intervention effects. The results showed that the mitigation facilities were effective, especially engineering efforts cooperating with vegetation revetments in the upstream area. The distribution patterns of erosion and deposition changed considerably by the intervention measures. Additionally, the effectiveness of each intervention scenario showed a gradual decline caused directly by the reduction of the reservoir capacity. Besides, the enhanced scenario functioned better than the present one with a smaller descent slope. The simulation methods assessed the ability and effectiveness of cooperated control measures and could support optimum mitigation strategies.

1 Introduction

Strong earthquakes trigger co-seismic landslides and crack the mountains discontinuously, increasing weak structural planes (Huang, 2009) by weathering and erosion. Consequently, the source materials produced from co-seismic landslides and attendant mass failure caused by the weak slope increase in mountainous regions and modify mountain landscapes by various surface processes for days, years, and millennia (Fan et al., 2020). The Wenchuan 2008 Ms = 8.0 (the surface-wave magnitude, which is the logarithm of the maximum amplitude of ground motion for surface waves with a wave period of 20 seconds) earthquake influences towns and other infrastructure in the affected area. Many studies have mapped the landslides triggered by the devastating earthquake. Gorum et al. (2011) performed an extensive landslide interpretation using a large set of high-resolution optical images and mapped nearly 60000 individual landslides, which are no less than 600m^2. Xu et al. (2014) delineated 197481 landslides formed by polygons, centroids, and top points compiled from visual image interpretation. To estimate the threat of loose materials in subsequent sediment disasters caused by landslides, some research attempt to measure the volume of deposited materials based on field survey and assumptions. Huang and Fan (2013) estimated 400 million m^3 of materials deposited in the heavy-affected areas by assuming that the materials deposited on steep slopes with angles larger than 30° and a catchment area more extensive than 0.1 km^2. An approximate 2793 million m^3 of sediment was calculated by Chen et al. (2009) using different deposited depth settings in different buffer zones of the fault. In summary, a tremendous number of loose materials are suspended on the gullies and hill slopes and ready to be eroded and transported away over a long time. Therefore, the mitigation is still in the long run in the Wenchuan quake-stricken area.

Structural mitigation measures have been developed in the affected areas regarding the site conditions and technical and economic feasibilities. For example, Ecological mitigation such as vegetation revetments was conducted to stabilize the source area in hillslopes (Cui and Lin, 2013; Forbes and Broadhead, 2013; Stokes et al., 2014), and check dams were used widely to intercept upriver sediment (Yang et al., 2021; Marchi et al., 2019). Lateral walls and levees were the longitude structures (Marchi et al., 2019) to protect the infrastructures in mountain watersheds with higher sediment supply to the main streams.

Although comprehensive mitigation measures were performed in potentially dangerous sites, disasters still occurred owing to rough terrain, vague source materials, intensive precipitation, and relatively low-cost mitigating measures (Yu et al., 2010; Cui et al., 2013). Therefore, understanding the effectiveness of intervention measures is crucial for mitigation strategies. More studies mainly focus on establishing post-evaluation effectiveness index systems that are not supported by sufficient practices (Zhang and Liang, 2005; Wang et al., 2015). Other research on long-term on-site measurement required more energy and financing and compared the changes before and after the intervention measures (Zhou et al., 2012; Chen et al., 2013). Recent research compares the disaster characteristics before and after the intervention, which are quickly obtained from the simulation (Cong et al., 2019; He et al., 2022). Nevertheless, the characteristics express the process ignoring the long-time effects on the geomorphic changes (longer than the duration of a single event). Therefore, the short-medium term (from the duration to decades) and spatial geomorphic changes quickly obtained from the simulation will provide more details to interpret engineering measures in notable locations, even in those inaccessible to humans.

The open access 2-D landscape evolution model CAESAR-Lisflood (C-L) is based on the Cellular Automata (CA) framework (Coulthard et al., 2013), which has powerful spatial modelling and computing capabilities to simulate complex dynamic systems(Batty and Xie, 1997; Couclelis, 1997; Coulthard et al., 2002). The model enables the study of many earth system interactions with different environmental forces. Representation of deposition and erosion within C-L is used widely in rehabilitation planning and soil erosion predictions from a post-mining landform (Saynor et al., 2019; Hancock et al., 2017; J.B.C.Lowry et al., 2019; Thomson and Chandler, 2019; Slingerland et al., 2019) and channel evolution and sedimentary budget with dam settings (Poeppl et al., 2019; Gioia and Schiattarella, 2020; Ramirez et al., 2020, 2022). In addition, there have been a series of studies in the mountainous area involving secondary geo-hazard driving factors (Li et al., 2018; Wang et al., 2014b) and vegetation recovery (Zhang et al., 2018). Li et al. (2020) and Xie et al. (2018) have used C-L with different rainfall scenarios or future climate change to interpret the landscape evolution after the Wenchuan earthquake. The methods and parameter values used in the above research helped to promote the application in other study areas.

In this study, we simulated and compared the geomorphic changes and sediment output in three scenarios that varied in mitigation compositions and intensities in a catchment. The objectives are to 1) assess the effectiveness of a set of mitigation facilities in reducing sediment transport, 2) analyse the role of each facility in geomorphic changes, and 3) determine vegetation influence on catchment erosion.

2 Study area

2.1 Regional characteristics

The study area was Xingping valley in the northeastern Sichuan province, a left branch of the Shikan river (a tributary of the Fu River) (Figure 1). There are nearly two hundred households scattered among more than five villages in the catchment. The topography of the catchment is rugged, with an elevation between 800 and 3036 m and an area of approximately 14 km^2. The catchment shape looks like a "leaf" with a nearly U-shaped main ditch characterised by a high longitudinal gradient (~ 120‰) and more than ten small V-shaped branch gullies. The length from northeast to southwest is 5770 m, the other direction perpendicular to which is 4150 m. A humid temperate climate with a mean annual temperature of 14.7℃ characterises the region. The mean annual precipitation is 807.6 mm, with maxima daily rainfall between May and September. The steep terrain and short-term heavy rainfall make an ephemeral stream in this area.

The local basement rocks are mainly metamorphic sandstones, sandy slate, crystalline limestone, and phyllite of Triassic Xikang Group (T_{3xk}) and Silurian Maoxian Group (S_{mx}), which quickly induce a large amount of loose solid material after weathering of a static process. Consequently, the Wenchuan earthquake that made this area one of the most severely affected locations with a Modified Mercalli Intensity scale of X (Wang et al., 2014a) produced 10^6 m^3 by triggering landslides from Mayuanzi, Zhengjiashan, and Wujiaping (Figure 1)(Guo et al., 2018).
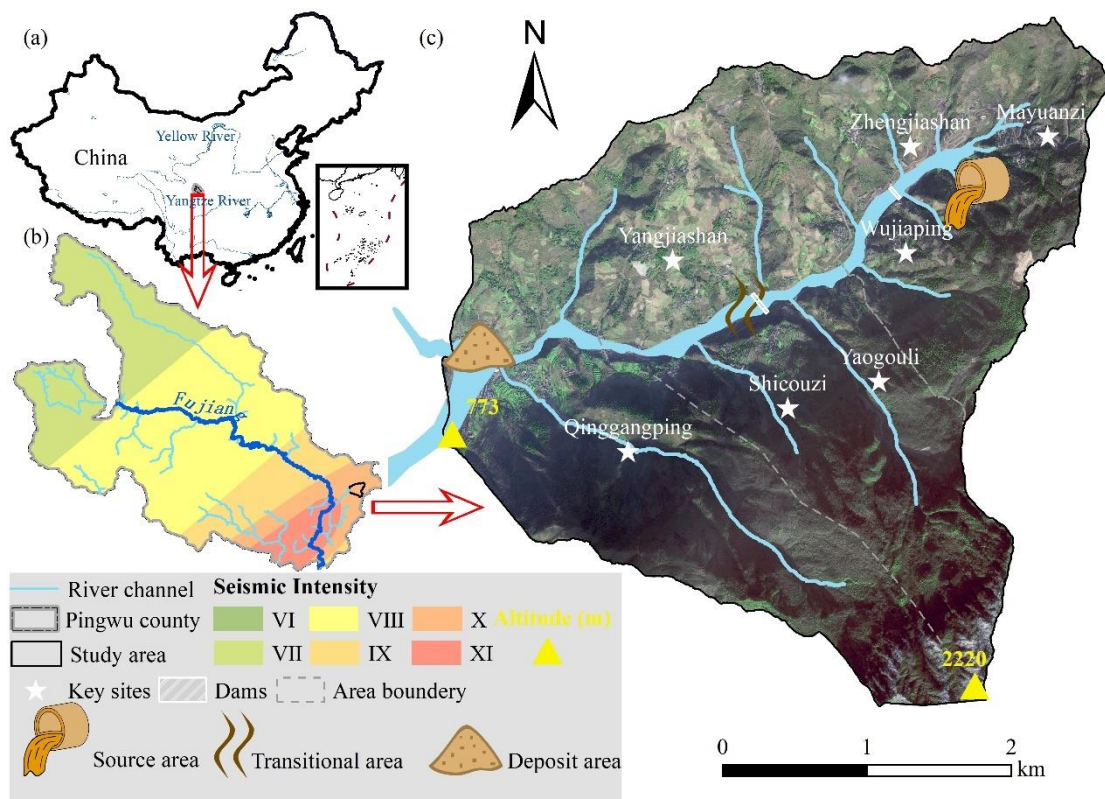
Figure 1: The location of the study area. (a) Location within China; (b) Location within the seismic intensity ranges of the Wenchuan earthquake and the Pingwu county; (c) The image of the area.

2.2 Historical hazards and intervention measures

Six group debris flow-flash flood disaster chains were found in Xingping valley decades after the earthquake. Based on the published work of SKLGP (State Key Laboratory of Geohazard Prevention and Geoenvironment Protection) and the local states' geological survey before 2018 and our biannual field surveys since 2012, we catalogued the time of occurrence, total rainfall of each event, corresponding disaster details in Table S1. The massive sediment was transported quickly after the devastating quake in 2008 and 2009. The extreme rainfall in 2013 and 2018 induced prosperous loose materials deposited in the channel. Considering the landslide processes, we divided the study area into three regions: source area, transitional area, and deposit area (the grey dashed lines in Figure 1c), which meant the loose solid materials would be easily transported from the source area to the deposit one through the transitional zone.

An engineering control project was completed to intercept the upriver materials in October 2010. The project included two check dams, one in the upper source area and the other in the transitional zone (Feng et al., 2017) (Figure 1c). The upper dam has a storage capacity of 5.78×10^4 m^3 and a height of 10.0 m. The transitional area dam has a storage capacity of 7.2×10^4 m^3 and a height of 9.0 m. With the reservoirs gradually filling with deposits, the first dredging work was subsequently done in 2013. Nearly three years later, the storage capacity behind the upper dam remained at 50% in 2016, while the transitional area dam cannot retain sediment.

3 Materials and Methods

In this study, we examined the intervention effectiveness through the morphological response and sediment yield in the Xingping valley, which was simulated using the C-L model. The research entailed four main steps: 1) setting three scenarios varied in intervention compositions, 2) preprocessing the input data including three groups of DEMs, the rainfall data, and m values of the C-L, 3) calibration of the hydrological component, and 4) simulating a three-year of the landscape changes and analysing the intervention effectiveness in 2011-2013.

3.1 Scenarios settings

The abundant source materials triggered by landslides should be controlled to prevent the threat of disasters downstream. Therefore, we designed three scenarios incorporating engineering and biological measures referenced to current facilities to assess the effectiveness of intervention measures. Scenario UP: Unprotected landscapes meant the sediments would transport without anthropogenic intervention. Scenario PP: Present protected landscapes implied that only the present two check dams trapped deposits in 2011-2013 without dredging work over the period (see section 2.2). Scenario EP: Enhanced protected landscapes emphasised the plus vegetation revetments in the source area and levees in the deposit area based on the two check dams in Scenario PP.

Figure 1c shows the locations of the existing two check dams in both Scenario PP and Scenario EP. We determined the placements of additional facilities in Scenario EP according to the field survey, which demonstrated the continuous supply of sediments was mainly from the source area. Therefore, the vegetation revetments like trees planting would be carried out upriver for their ability to prevent erosion by stabilising topsoil and enhancing the soil's infiltration capacity with its roots (Lan et al., 2020).

Considering that the flash-flood gushed in and damaged the residential area downriver (see Fig. 2 and Section 3.2.2), the levees are artificial barriers to protect agricultural land and buildings, which helped to prevent the mixture of water and sediment from overflowing and flooding surrounding areas. We simulated and compared the three types of situations described above.

3.2 CAESAR-Lisflood

The C-L model integrated the Lisflood-FP 2D hydrodynamic flow model (Bates et al., 2010) with the CAESAR landscape evolution model (LEM) (Coulthard et al., 2002; Van De Wiel et al., 2007), which is entirely described in Coulthard et al. (2013). We used the catchment mode that required the surface digital elevation model (DEM), the bedrock DEM, the grain size distribution, and a rainfall time series to simulate the sediment transport and geomorphological changes in this study. The four primary modules operate as follows:

(1) a hydrological module generates surface runoff from rainfall rates using an adaption of TOPMODEL (Topography based hydrological model) (Beven and Kirkby, 1979),

(2) a hydrodynamic flow routing module based on the Lisflood-FP method (Bates et al., 2010) calculates the flow depths and velocities,

(3) an erosion and deposition module uses hydrodynamic results to drive fluvial erosion by either the Einstein (1950) or the Wilcock et al. (2003) equation applied to each sediment fraction over nine different grain sizes,

(4) and a slope model eliminates materials from the slope to the fluvial system when a critical slope threshold is exceeded.

The C-L model updates variables in square gridded cells at intervals, such as DEM, grain size and proportion data, water depth, and velocity. For three scenarios, the initial conditions, such as DEMs and bedrock DEMs, the rainfall data, and the m values were reprocessed as follows.

4

3.2.1 Surface and bedrock digital elevation model

Although the run time of the C-L simulation increases exponentially as the number of grid cells increases, to describe clearly the control process, especially the two dams and levees in the catchment, we unified grid cell scales to 10 m for all needed data. The GlobalDEM product with a 10 m × 10 m resolution and 5 m (absolute) vertical accuracy was used as the prepared data to form three types of initial DEMs (UP DEM, PP DEM, and EP DEM). Before rebuilding initial DEMs, we filled the sinks of the original GlobalDEM based on Environmental Systems Research Institute's (ESRI's) ArcMap (ArcGIS, 10.8) to eliminate the 'walls' and the 'depressions' in the cells and avoided the intense erosion or deposition in the early run time. Then the non-sinks DEM was used as the surface DEM in Scenario UP (UP DEM) without any facilities. According to the engineering control project described in Section 3.2.2, Scenario PP's surface DEM (PP DEM) included the dams by raising the grid cell elevations by 10 m for the upper dam and 9 m for the dam in the transitional area. Similarly, the surface DEM in Scenario EP (EP DEM) included the dams in PP DEM. In addition, two levees were produced by raising grid cells' elevation by 2 m that were represented at selected locations. Incidentally, the placement and setting of vegetation revetments in Scenario EP were introduced in Section 3.2.2.

In Section 2.2, the spatial heterogeneity of source materials indicates the discrepancy of erodible thickness, which equals the difference between surface DEM (DEM) and bedrock DEM (bedDEM). We divided the erodible thickness into five regions (Fig. S1) by checking out the relative elevation of the foundations of buildings, the exposed bedrock, and the deposited depth of landslides to the ground level. The average thicknesses of upstream low and high-altitude areas were set to 10 m and 3 m, respectively, and the erodible layer in the downstream area was 3 m. For the river channel and outlet, there would be a large amount of deposition, and the thickness of erodible sediment was set to 5 m and 4 m, respectively. The dams in Scenario PP and the levees in Scenario EP were non-erosive concrete. As such, we set the erodible thickness of these features to 0 m. Eventually, DEMs were formatted to ASCII raster as required by C-L. The divided regions varied in erodible thickness, the placement of additional levees and vegetable revetments in Scenario EP, and the generation process of DEMs and bedDEMs were shown in Fig. S1.

3.2.2 Vegetation settings

Another parameter required in each scenario was the m value in C-L's hydrological model (TOPMODEL), which controls the exponential decline of transmissivity with depth (Beven, 1995, 1997) and influences the peak and duration of the hydrograph in response to rainfall. The lower the m value, the lower the vegetation coverage, and the flashier flood peak and shorter duration are reflected in the flood hydrograph (Coulthard et al., 2002). The m value is usually determined by the landcover (e.g., 0.02 for the forest, 0.005 for the grassland) (Coulthard and Van De Wiel, 2017). In our study, we set the value as 0.008 in our smaller catchment (14 km^2) in Scenario UP and PP, which resembles the m value of farmland covered with lower vegetation in the same catchment studied by Xie et al. (2018) and Li et al. (2018). As mentioned earlier, the upstream-low elevation area covered by the biological measures designed in the EP scenario was assigned a higher m value of 0.02. It has been calibrated in the more extensive catchment containing our study area by replicating the flood event in 2013 (Xie et al., 2018).

3.2.3 Rainfall data

In this research, we compared three scenarios with identical precipitation data between 2011 and 2013, as mentioned in section 3.1. The source data of precipitation in 2011-2013 (Figure 2a) was from the China Meteorological Administration (http://data.cma.cn) with daily temporal resolution. The rainfall intensity and the frequency of extreme events affect patterns of erosion and deposition (Coulthard et al., 2012b; Coulthard and Skinner, 2016). Therefore, we used the stochastic downscaling method to generate hourly data to best capture the hydrological events in this study, which was introduced by Li et al. (2020) and Lee and Jeong (2014). The referenced hourly precipitation was from the pluviometer located 20 km from the study

area in 2016 (Figure 2b), with an annual total precipitation of 684 mm. The rainfall in 2016 was characterised by that (1) hourly precipitation was from 1.1 mm to 35.4 mm, and (2) the maximum and average duration of a rainfall event was 24 h and 2.8 h, respectively. The main processes of the downscaling method are:

- extracting the hourly rainfall of specific days in 2016 closest to the daily rainfall in 2011-2013 through the threshold setting and producing the genetic operators using the extracted hourly rainfall dataset;

- mixing on the genetic operators by genetic algorithm (Goldberg, 1989) composed of reproduction, crossover and mutation and repeating until the distance between the sum of hourly rainfall and the actual daily rainfall is less than the set threshold;

- normalising the hourly precipitation to remain the daily rainfall value unchanged. The input of generated hourly precipitation is catchment lumped in Scenario UP and PP and divided into two separate but identical rainfall in Scenario EP.

Figure 2c shows the downscaled rainfall series between 2011 and 2013. The downscaled hourly precipitation better captured the hydrological events on account of the hourly-mean rain (5.27 mm) in the day with extreme rainfall (126.5 mm), which was far from the actual situation.
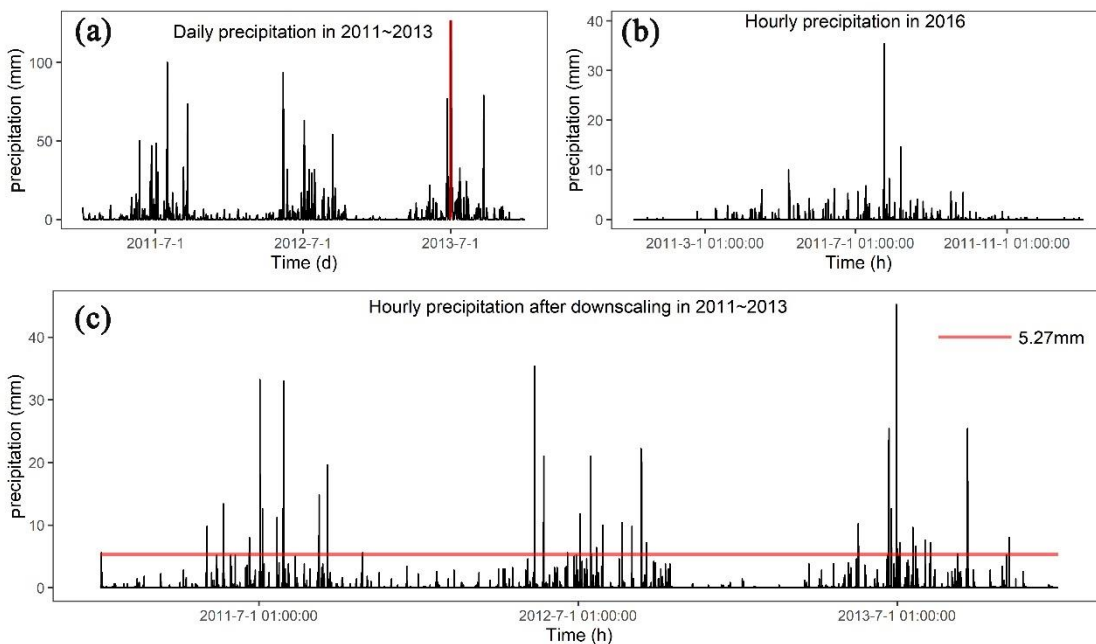
Figure 2: (a) Daily precipitation in 2011-2013 (the red vertical line indicates maximum daily precipitation of 126.5 mm); (b) Hourly precipitation in 2016; (c) Downscaled hourly precipitation in 2011-2013 (the red horizontal line indicates the hourly-mean precipitation 5.27 mm in the day with maximum precipitation showed in (a)).

3.2.4 Other parameters

The C-L model is sensitive to a set of input data introduced by Skinner et al. (2018) for a catchment with a grid cell size of 10 m, such as sediment transport formula, slope failure threshold, and grain size set. The grainsize distribution of sediment is derived from samplings at 14 representative locations in the same study basin by Xie et al. (2018). Given the grainsize distribution in this study, we selected the Wilcock and Crowe formula as the sediment transport rule, which was developed from flume experiments using five different sand-gravel mixtures with grain sizes ranging between 0.5 and 64 mm (Wilcock et al., 2003). Considering the steep slope on both sides of deep gullies there distribute, we tended to set a higher slope failure threshold to replicate the geomorphic changes between 2011 and 2013 realistically. Additionally, we found that the probability of shallow landslides indeed accumulated from 20° to 50° in slope gradient between 2011 and 2013 (Li et al., 2018). The slope angle was derivate from the DEM with a 30 m spatial resolution, which caused a lower slope angle than that with a 10 m resolution. As such, we set 60°, which is lower than the 65° used in a scenario without landslides (Xie et al., 2022) and higher than 50°. Some parameters were determined by repeated experiments such as the minimum Q value and the other input values were referred to default values recommended by the developers (such as the max erode limit in the erosion/deposition module

and the vegetation critical shear stress) in https://sourceforge.net/p/caesar-lisflood/wiki/Home/.Table S2 in the supplemental material presented C-L model parameters used in the current study.

3.2.5 Model calibration

Considering the ungauged basins before 2015, we replicated the flash flood event in July 2018 by C-L to calibrate the hydrological components. Based on Scenario PP (with two check dams), we changed the rainfall series into the two-week hourly precipitation in July 2018 (Fig. S2a), which is recorded by the rain gauge 2.5 km away from the catchment (Fig. S2b). The simulation results (Fig. S2c and Fig. S2d) represented the erosion map and maximum water depth map in Scenario PP on July 15, 2018. As shown in Fig. S2c and Fig. S2d, we selected three locations to compare the simulation results with remotely sensed images and photos. The comparative results (Fig. S3) revealed the similar ranges of the deposition and inundation between simulation results and remotely sensed images. Additionally, the values of simulated sediment depth and water depth were close to those measured from images, which indicated that the flash flood event was replicated successfully by the C-L using the input data.

Table 1 shows three-year landscape changes under three different scenarios that were simulated and compared to analyse the intervention effectiveness in 2011-2013.

Table 1: Scenarios setting

Scenario	Descriptions	Period	DEM (10m)	Rainfall data
UP	no anthropogenic intervention		UP DEM UP bedDEM	downscaled hourly precipitation in the period (lumped)
PP	the present two check dams upstream without dredging work	2011-2013 (3 years)	PP DEM PP bedDEM	
EP	additional vegetation revetments in the source area and levees in the deposit area based on Scenario PP		EP DEM EP bedDEM	downscaled hourly precipitation in the period (spilt)

3.3 Output analysis

The C-L model outputs in each scenario include hourly discharge at the basin outlet, the difference between DEMs at a specified time and initial DEMs (EleDiffs), and hourly sediment yield. We validated the model outputs by comparing the hourly discharge and EleDiffs reflecting the depth of sediment deposition or erosion (> 0.1 m: deposition, < 0.1 m: erosion) with field survey materials. The overall temporal and spatial geomorphic changes reflected by EleDiffs under three different scenarios were used to assess the geomorphic response to interventions. To explore the response to various control measures, we zoomed in on the key spots placed checking dams, levees, and vegetation revetments and recorded the depth of deposited sediment behind two dams. For further exploring the spatial heterogeneity, we compared respectively with the volumes of deposition and erosion in three divided regions, including the source area, transitional area, and deposition area.

Based on the visual and quantitative results, we defined two formulae to assess the intervention's effectiveness. The conservation ability (Ca, Eq. (3)) was based on variables in the sediment balance system (Figure 3). The sediment volume of deposited sediment (D_n) and input sediment from the upper connected region (I_n) is equal to that of eroded material (E_n) and output sediment to the next part (O_n) over the same period (Eq. (1), Eq. (2)) in the system. A higher value of Ca in a specific region and scenario indicates that a more effective control system is applied.
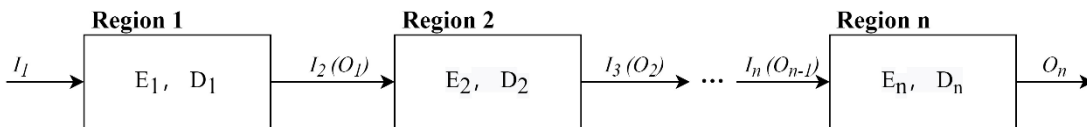
Figure 3: The sediment balance system in the study area (the Region n indicated source area, transitional area, and deposit area in this study)

$$I_n = \sum_{2}^{n} E_{n-1} - \sum_{2}^{n} D_{n-1},$$ (1)

$$I_n + E_n = O_n + D_n,$$ (2)

$$Ca = \frac{D_n}{I_n + E_n}$$ (3)

244 Where, n is the region number of source area (=1), transitional area (=2), and deposit area (=3).

245 Additionally, we designed the relative efficiency (Re, Eq. (4)) to depict how much a set of intervention measures in Scenario

246 PP and EP were efficient in sediment loss, with the comparison to Scenario UP.

$$Re_{PP/EP,i} = \frac{Q_{UP,i} - Q_{PP/EP,i}}{Q_{UP,i}}$$ (4)

247 Where i is the sequence of the day; Q_{UP} is the daily sediment yield measured at the catchment outlet in Scenario UP; $Q_{PP/EP}$ is

248 the daily sediment yield measured at the catchment outlet in Scenario PP or Scenario EP of day i; $Re_{PP/EP}$ is daily relative

249 effectiveness of control measures in Scenario PP or Scenario EP.
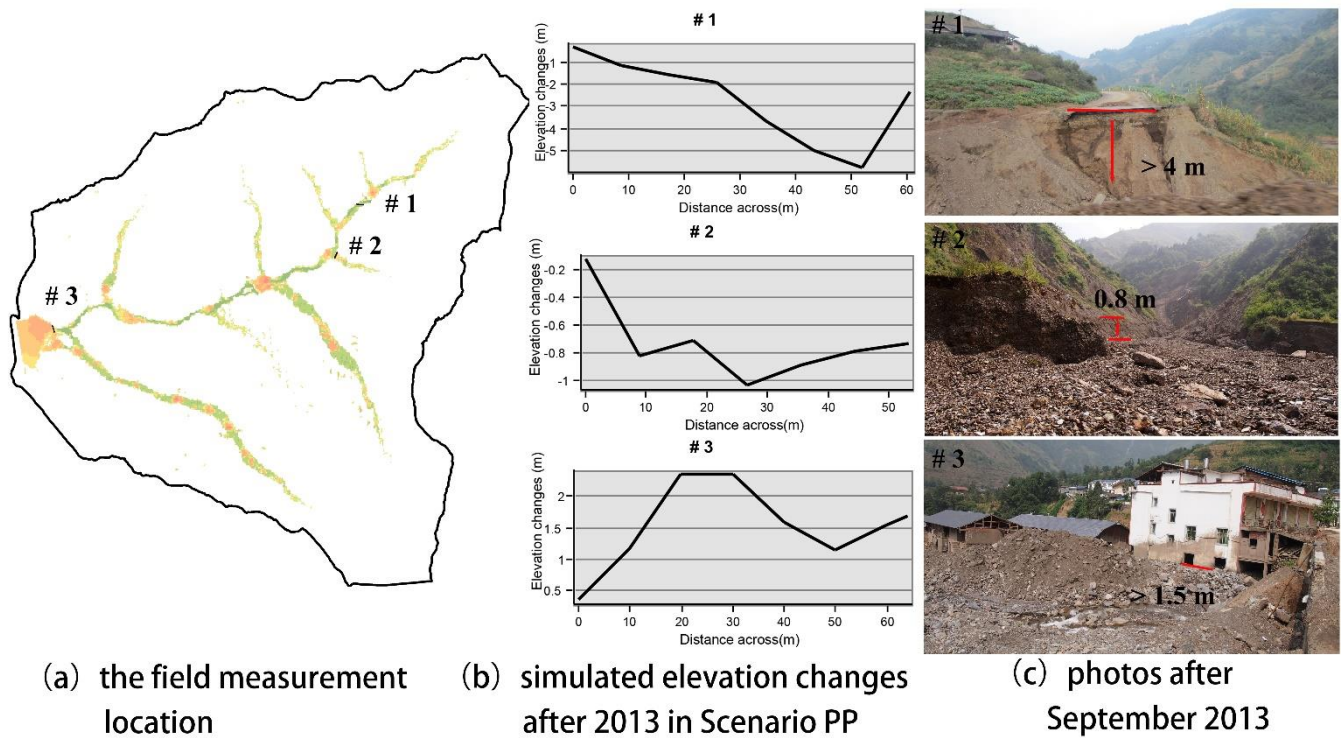
4. Results

4.1 Model verification

252 Figure 4 shows the input precipitations and modelled discharge hydrograph between 2011 and 2013 (Figure 4a), in addition,

253 presents the comparison of simulated mean discharge in April through July and the whole year with field survey materials in

254 two locations (Figure 4 b, c). Concerning the discharge hydrograph, the peak discharges (63.7, 54.9, and 50.3 m³/s) appear

255 identically with the peak rainfall intensities (31, 19.7 and 15 mm). The value of modelled discharge from March to May in the

256 catchment outlet (location A) is slightly larger than the measured value recorded by Feng et al. (2017). Additionally, an average

257 annual discharge of 10.04 m³/s in location A is less than that of 12.80 m³/s in the catchment outlet (location B), which has an

258 area approximately three times the study area.
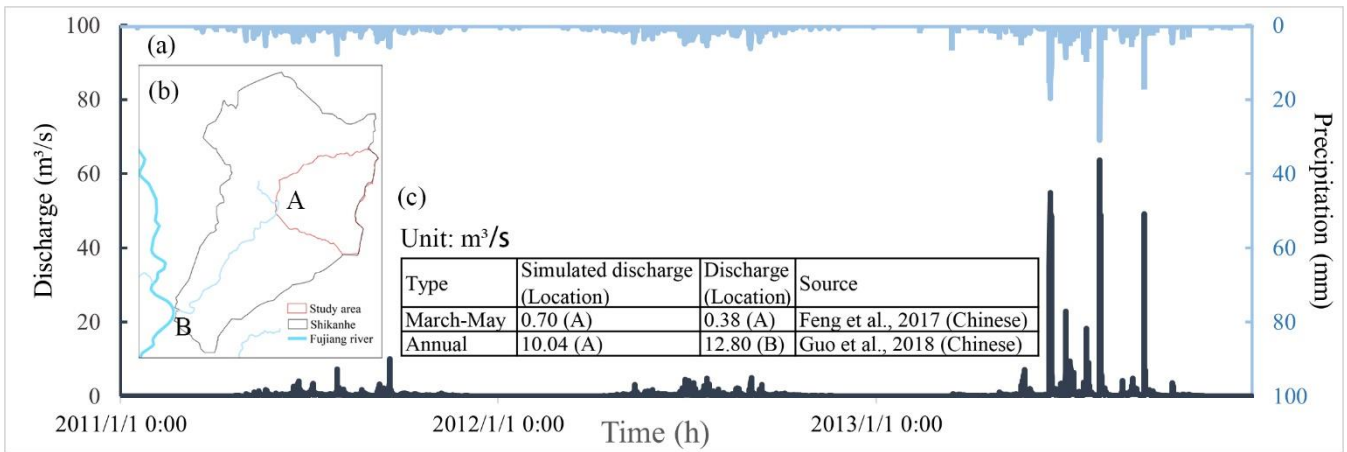
260 **Figure 4: (a) The input hourly precipitation and simulated discharge in 2011-2013 in Scenario PP; (b) the specified locations to verify;**
261 **(c) the comparison of the simulated average discharge to the recorded discharge.**

262 Figure 5 compares typical cross-sections to the site photos based on the replicated landscape changes in Scenario PP. The first

263 site is on the upriver road, which was eroded to a depth of 5 m according to the simulation results, while the photo shows a

264 depth of no less than 4.0 m without an apparent eroded base. The cross-section and site photo of the gully labelled 2 depict

that the eroded depth is approximately 1.0 m. Meanwhile, a clear sediment boundary is found in the building located at the deposited area, indicating a slightly lower deposition depth than the modelled one.


(a) the field measurement location   (b) simulated elevation changes after 2013 in Scenario PP   (c) photos after September 2013

Figure 5: The comparison of cross-sections from the simulation results to the photos in the field measurement locations after 2013 in Scenario PP.

4.2 Overall geomorphic changes

Figure 6a shows the three annual landscapes changes in each scenario, which were classified into seven ranks by natural breaks for EleDiffs: extreme erosion (<-7 m), heavy erosion (-7--3 m), moderate erosion (-3--1 m), light erosion (1-0.1 m), micro change (-0.1-0.1 m), light deposition (0.1-1 m), moderate deposition (1-3 m), heavy deposition (3-7 m), and extreme deposition (>7 m). A similar spatial pattern of erosion is observed in all three scenarios. In detail, erosion occurred mainly in the main channel and the branches on both sides, among which the left branches were severe. In contrast, the deposition distribution appeared to be varied in three scenarios, especially behind the two dams showed in Scenario PP and EP.

The total area of affected grid cells representing erosion and deposition in each scenario was calculated to reveal the difference (Figure 6b). As shown in Figure 6b, the affected area in Scenario UP was the largest at about 0.76 km^2 (5.4% of the total catchment), which was larger than that in Scenario PP (0.70 km^2, 5.0% of the whole catchment), and the area decreased to 0.61 km^2 (4.4% of the total catchment) in Scenario EP. The total area of erosion and deposition reduced gradually as more controlling measures were established in this study.

Figure 6c compares the extent of geomorphic changes in three situations using the areas varied in depth. Erosion in the three scenarios was similar in that the light and moderate erosion areas were more than the extreme and heavy erosion areas. The area of each erosion degree in UP was more extensive than in PP and larger than in EP. In addition, the greater the deposition depth, the less deposition coverage. Especially the extreme deposition area was somewhat more than the area of the heavy deposition in UP. Further analysis shows that extreme, moderate, and light deposition areas decreased in the order of UP, PP, and EP. The heavy deposition areas show the opposite trend, mainly contributing to the checking dams and vegetation revetments.

9
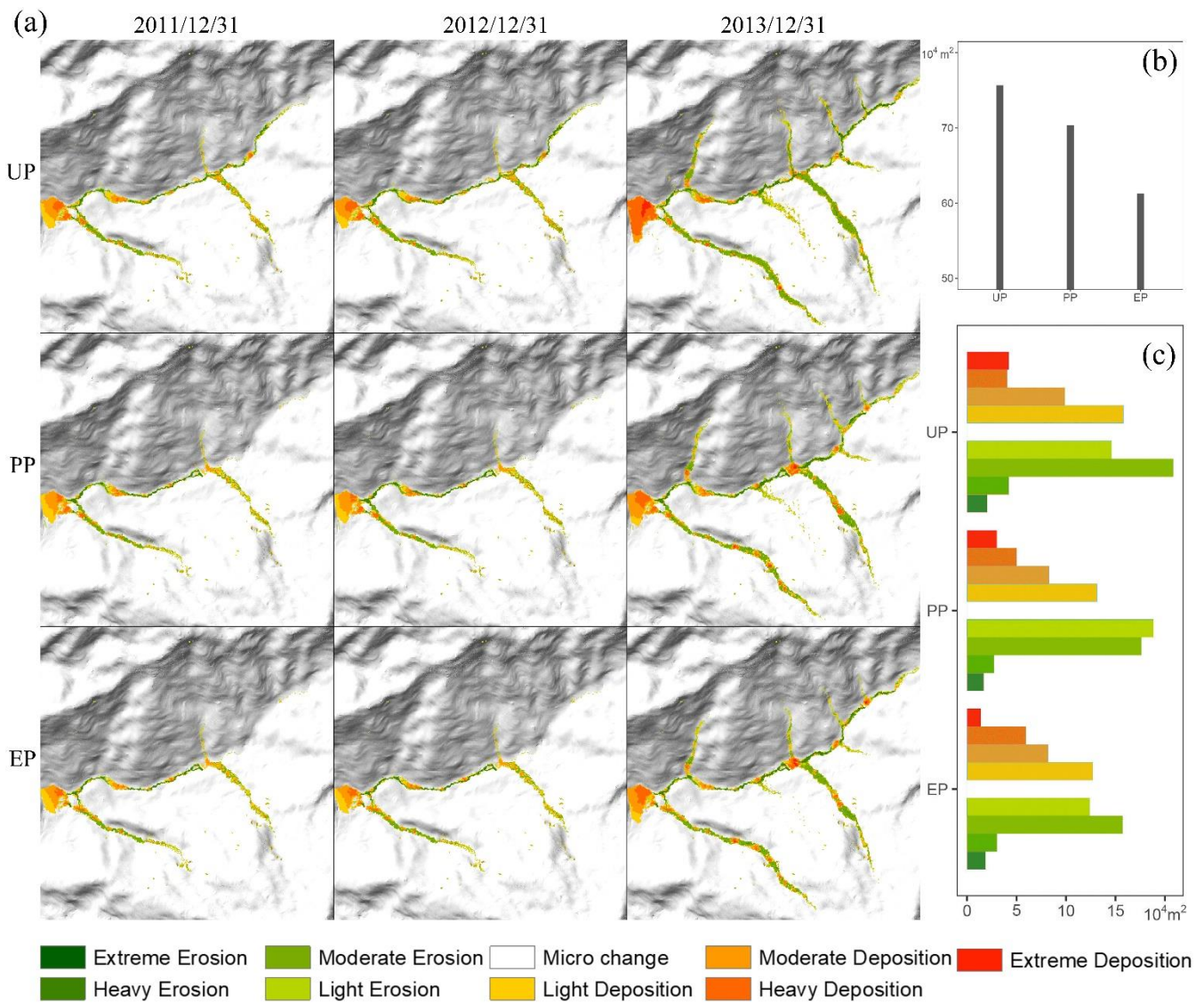
Figure 6: (a) Simulated internal geomorphic changes over time for three scenarios; (b) the affected area included deposition and erosion for three scenarios; (c) the ranks of deposition and erosion for three scenarios.

4.3 Details of key spots

As shown in Figure 7, we provide a detailed investigation of the controlling measures and surroundings for the three scenarios. Behind the two dams upriver, the evident orange clusters indicate that the deposition appeared in Scenario PP and EP. In contrast, these locations were dominated by erosion, shown in green in scenario UP. Further analysis of the sediment depth shown in Figure 8 showed that the values of deposited depth behind the dams in Scenario EP were lower than those in Scenario PP. Additionally, in Scenario PP, sediment trapped by dam 1 was lower than that by dam 2, but both with more than 10 m-deposition exceeded the dams' heights (the dam 1's height is 10 m, the dam 2's height is 9 m) finally. At the conclusion of the simulation in Scenario EP, the values of depth behind the two dams were nearly 8 m, which were lower than the dams' heights. The materials produced from upriver tributary gullies varied by the additional biological protection measures in three scenarios. A volume of 14.4×10^4 m^3 sediments was transported from EP's biological protection area (solid lines in Figure 7). The loose materials were 27.1×10^4 m^3 and 16.9×10^4 m^3, respectively, were produced in the same region without biological protection in Scenario UP and PP. The vegetation revetment enhance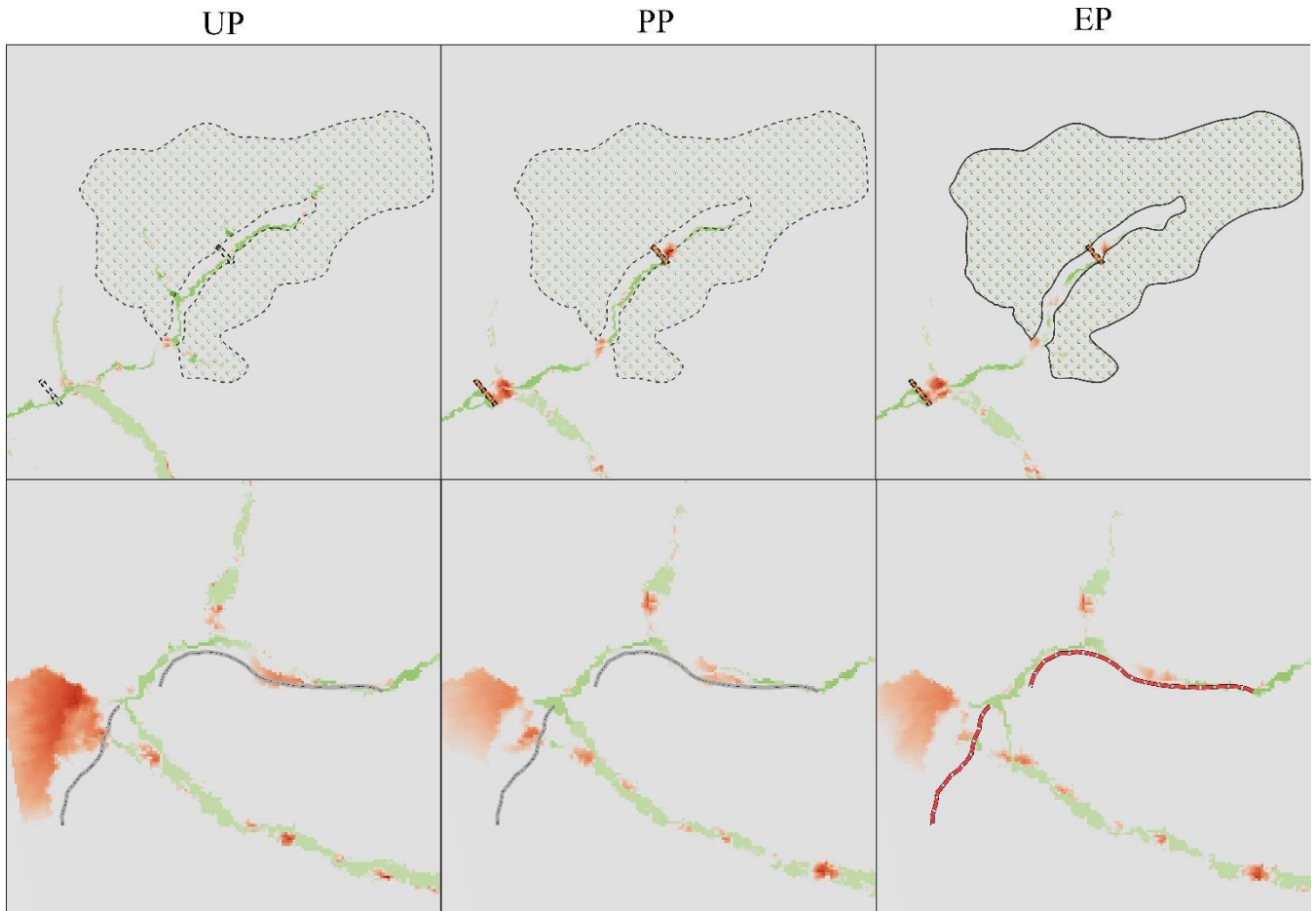d the sediment conservation based on the role of dam 1. Compared with the deposition in UP and PP without levees in the downriver area shown in the bottom row of Figure 7, the levees in EP blocke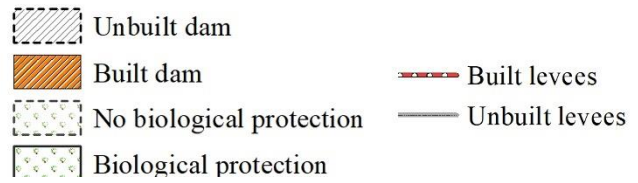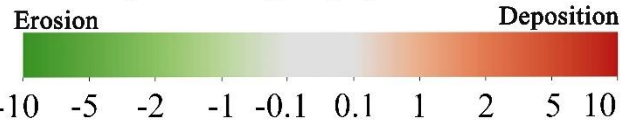d debris in the bend of the channel and played an essential role in protecting the residents and cultivated land behind the levees.
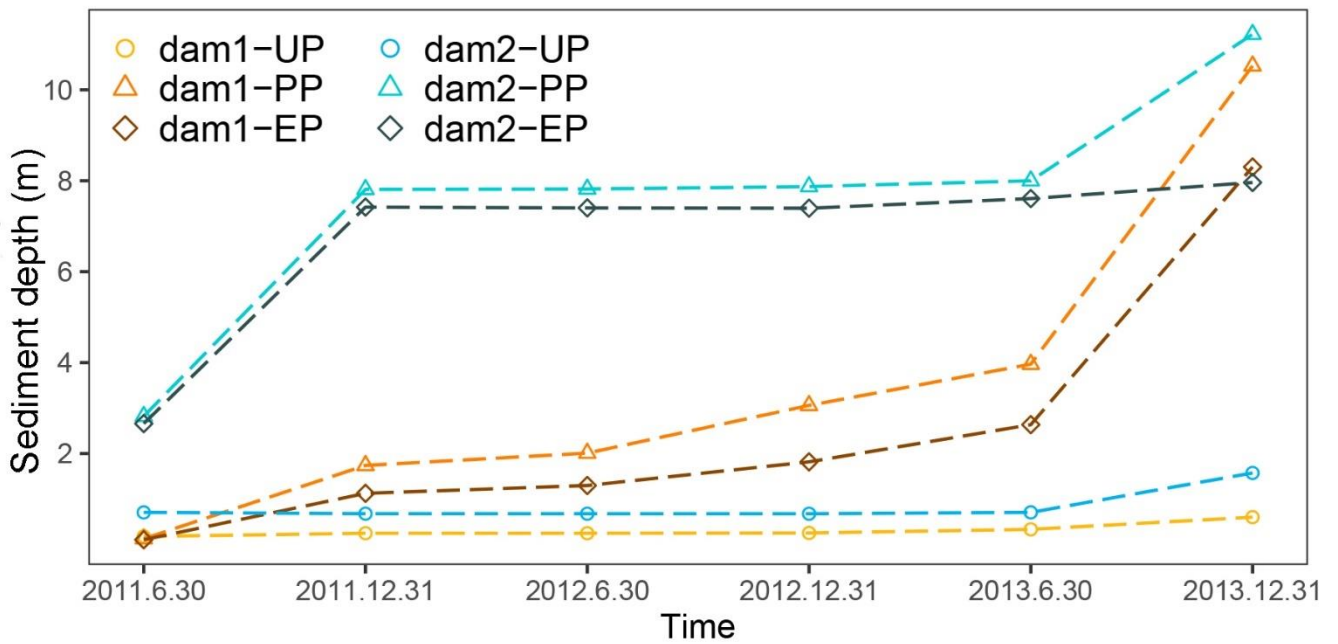
Figure 7: Geomorphic changes at the conclusion of the simulation at key spots for the UP, PP, and EP scenarios. The top row is the upriver section containing dam 1, dam 2 and the vegetation revetment. The bottom row is the downriver section containing levees.


Figure 8: The depth of deposited sediment in the dams' placements.

4.4 Effectiveness assessment

Figure 9 shows the erosion and deposition volumes in the source, transitional, and deposit areas and compares *Ca* in each scenario. The data showed similar phenomena in three scenarios. For example, the deposition volume in the source area was less than that in the transitional area, and the largest amount of sediment was deposited in the deposit area. Regarding the eroded sediment, the largest volume was in the transitional area, and the least was in the source area. Moreover, sediment transport could be controlled the best in the deposit area and the worst in the source area in any intervention conditions.

By comparing the *Ca* of the source area in Scenario UP, the value was increased by 138.1% in Scenario PP, which was responsible for the dam1. And then dam 2 in the transitional area reduced sediment loss effectively reflected by the 52.5% increase in *Ca*. Furthermore, the mitigation measures in Scenario PP with vegetation revetment and levees in Scenario EP worked better. The conservation ability in the source area increased by 161.9%, and the levees helped increase by 3.49% in the deposit area. Therefore, the dams are most effective in blocking sediment. The vegetation revetments strengthen the conservation ability, while the levees are helpful but with a discernable impact on sediment conservation.
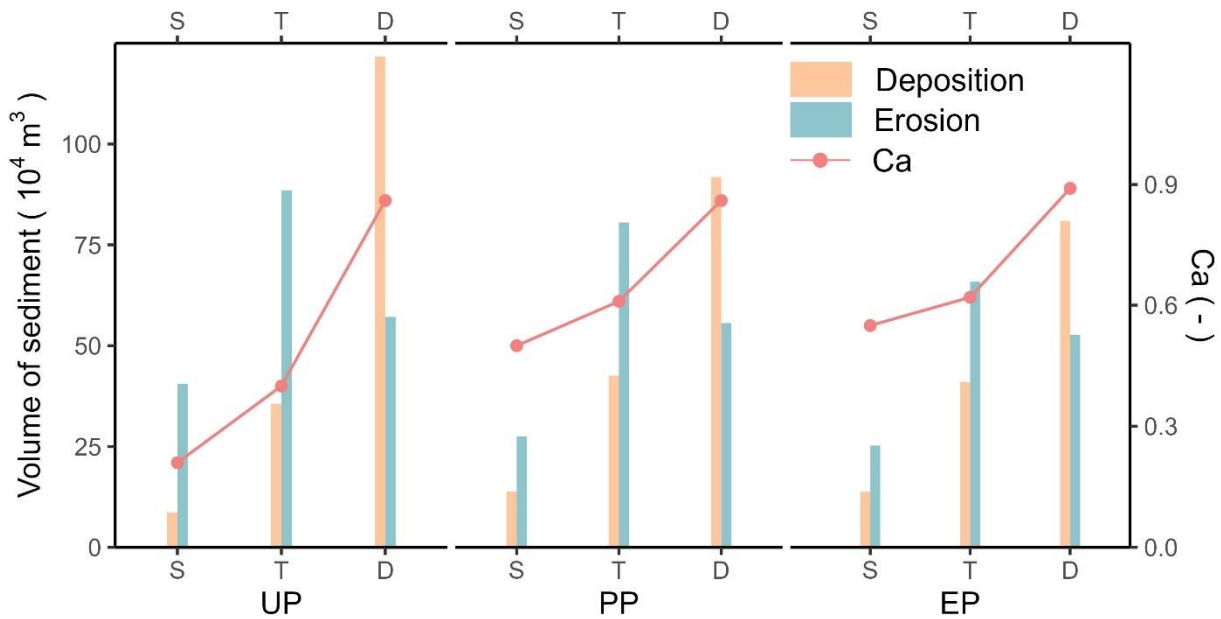
Figure 9: The volumes of sediment and the conservation ability (*Ca*) in three areas in each scenario (S: source area; T: transitional area; D: deposit area.).

Figure 10 presents the cumulative sediment yield time series for each scenario and the relative efficiency of scenario UP and EP. The steep curve of output cumulative sediment means a significant increase of deposition, and three increasing stages have high consistency with the rainfall intensity in three monsoons (May-September). The total sediment output in UP was the largest, about 30.4×10^4 m^3, and the total production in PP (26.3×10^4 m^3) was larger than that in EP (19.3×10^4 m^3).

The relative efficiency over the period of controlling measures by human intervention in PP and EP (Figure 10b) indicates three distinct stages. Stage I shows that the intervention measures in both scenarios prevented the sediment transport completely. Later stage II is a peculiar period when the effect of enhanced protective measures in EP was not as good as that in PP through repeated experiments, which the increasing complexity of the model would cause. In stage III, the relative efficiency of the intervention measures in EP was greater than that in UP, which could achieve long-term effect and stable conservation of solid materials.

12
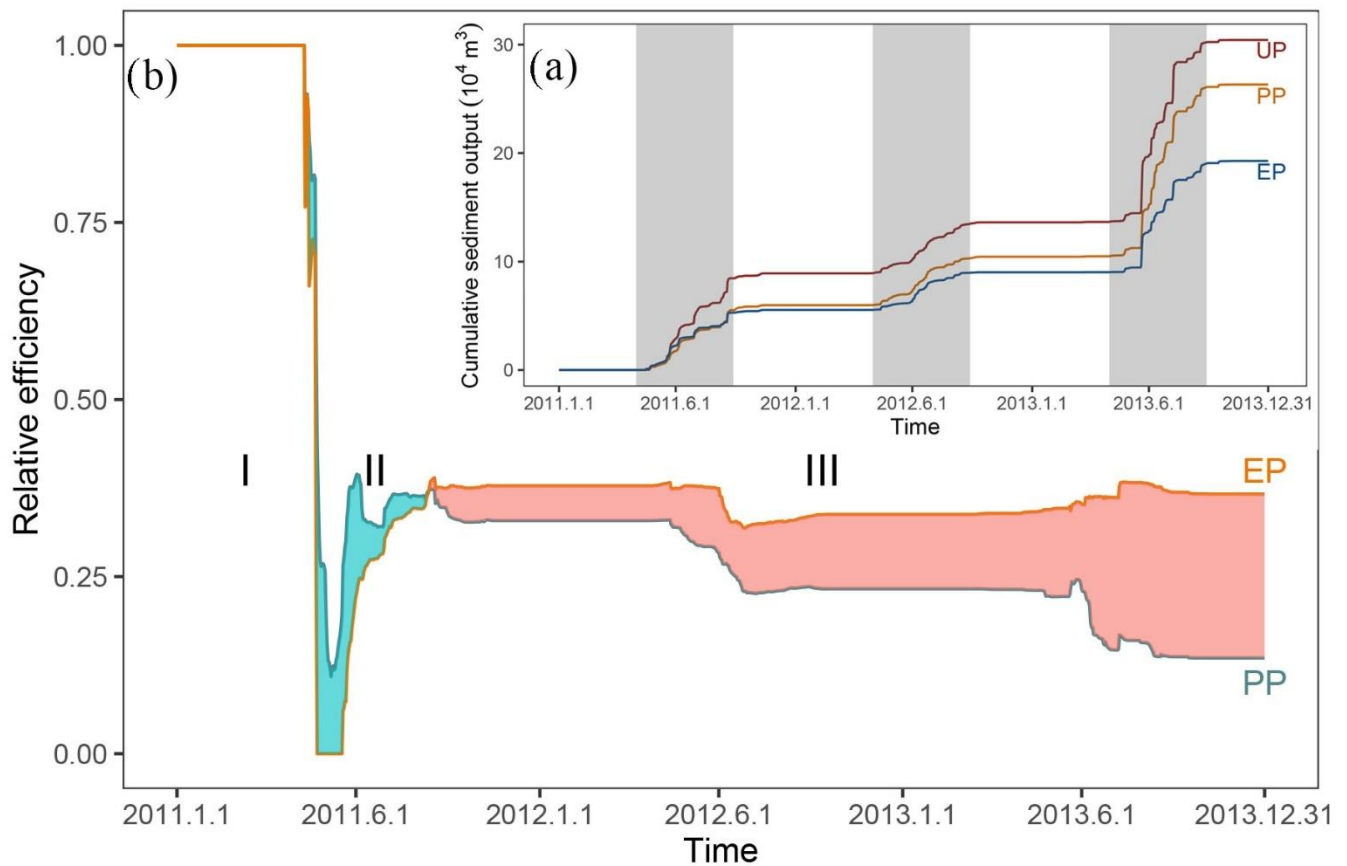
Figure 10: (a) showing the cumulative output sediment over time (grey region highlighting three monsoons), (b) showing the relative efficiency of scenario UP and EP compared with the UP (cyan shading represents when PP is more effective than EP and red shading represents the opposite)

5. Discussion

5.1 Model uncertainty and application

Uncertainty deserves a discussion for understanding and implementing the simulation results in most geographical analyses and modelling processes (Yeh and Li, 2006). Comparative simulation tests using the C-L tool suggested a complex spatial and temporal evolution of sediment transport. They demonstrated that the efficiency varied in scenarios, which differed in control measures conducted on the mountainous areas susceptible to secondary geo-hazards. In this study, we cited local research and comprehensive parameter sensitivity papers for the parameters involving geological conditions. We downscaled the daily rainfall sequence into hourly data collected in 2016 for every year because the total rainfall and intensity were identified as a 'normal year' in 2016 (Xie et al., 2018). Although the intensity and event time would not be the same as the actual value for the generated input data, the realisation of total rainfall in three different years suggested reasonable differences.

The methods applied in the study further demonstrate the role of C-L as a tool to understand the short-medium term or long-term geomorphology changes (Ramirez et al., 2022; Li et al., 2020; Coulthard et al., 2012a) and observe the effectiveness of natural hazard interventions measures provided different rainfall patterns. For example, the mitigation facilities in this study were effective, especially engineering efforts cooperating with vegetation revetments in the upstream area, which would help decision-makers to optimise the management strategies to control mountain disasters. Geotechnical engineering has disadvantages, even though it is a mature technology that identifies and fixes problems quickly (Cui and Lin, 2013), such as the greater work and expense and the difficulty of maintenance. While the 'green development', the vegetation cover was effective in preventing erosion by strengthening topsoil and absorbing excess rainwater with its roots (Reichenbach et al., 2014; Stokes

et al., 2014; Forbes and Broadhead, 2013; Mickovski et al., 2007). Alternatively, the methods could be used to study the tree planting patterns on different slopes.

5.2 Short-medium term problem

We used an ingenious and simple method to build the dams and levees in the simulation by increasing the elevation in the expected location and assuming that it could not be eroded (see https://sourceforge.net/projects/caesar-lisflood/). This method proved to be experimentally feasible (Gioia and Schiattarella, 2020; Poeppel et al., 2019). The rigid dam and levee body embedded in the model would not be broken, and the effect would not weaken, so the result of the geo-hazard risk assessment would be reduced to some extent. Although the short and large number of moving debris triggered a tremendous impact in the simulation, the tools could not simulate the geo-hazard chain links. They would ignore the fierce attack on the environment and facilities downstream. Some typical geo-hazard chains were focused on the specified event in a short time and recreated the hazard lifecycle using physical and mechanical models (Fan et al., 2020). We concentrated on the effectiveness of mitigation measures in the short-medium term, which is different from those in space-time scales and purposes. Therefore, the three-year simulation time made it underestimated risk assessment and success to simulate the effect of mitigation measures compared with the actual result in this study.

5.3 Sediment transport patterns

Unlike the typical debris flow research, where three divided areas get their names for the materials process, the simulation result demonstrated that the loose solid materials from the source area sliding to the resting area were the least among the three regions, even for the scenario UP (unprotected landscapes). The sediment transport patterns change considerably. First, the abundant loose solid materials formed by the strong earthquake have stabilised generally since 2008's debris flow (details in Table S1). Second, the long and deep gullies are mainly located in the transitional area (Yaogouli, Shicouzi, Yangjiashan) and deposit area (Qinggangping), which provide more sediment supply than the source area. As shown in Fig. S4, the movement of the materials occurred mainly in the branches in the transitional and deposit area. Moreover, the mitigation measures intervened in surface process, which lead to the changes in erosion and deposition in three areas. For example, an increase of deposition and a reducing of erosion appeared to be in source and transitional area, while the sediment deposition reduced significantly in deposit zone.

5.4 Long-term effectiveness

In the warmer world, with more water vapour in the atmosphere, precipitation extremes will intensify, increasing the likelihood of extreme and intense rainfall (East and Sankey, 2020). Then sequential increased fluvial transport capacity and erosion would accelerate geomorphic changes. With increased uncertainty of precipitation and temperature, future work on the landscape evolution of three scenarios will help to understand the long-timescale effectiveness of intervention measures. We randomly selected one of the 50 repeat datasets downscaled by Li et al. (2020), which were generated in 2013-2025 and RCP 4.5 emission scenario from NEX-GDDP (spatial resolution: 0.25°×0.25°, temporal resolution: daily) to simulate the effectiveness in three scenarios. The result (Figure 11) illustrated that stage III (the stable stage that started on the 161st day, in which Scenario EP's intervention measures were more effective) was more than stages I and II, which were only in the beginning. The relative effectiveness in both scenarios decreased gradually, and the curve went down faster in PP than in EP.

We further explain the change in intervention effectiveness over time. The effectiveness of controlling sediment transport is primarily for two reasons. The first one concerns the sediment trapping capability of checking dams and the increase of soil's infiltration capacity with vegetation roots. Another is because of the positive feedback about the geomorphic changes, especially the deposition behind the dams. Because the gradient of the upriver channel is slowed down by checking dams, and the sediment carry capacity from the flow is reduced (Luan et al., 2022; Hassanli and Beecham, 2013). The storage capacity of

14

checking dams fades as the accumulation of sediment deposits, which necessarily lead to the gradual decrease of intervention effectiveness. Additionally, the vegetation revetments still reduce sediment transport by stabilising topsoil over the period when the reservoirs are filling with sediment without dredging work. Therefore, the effectiveness of compound measures in Scenario EP goes down with a gentler downward trend.
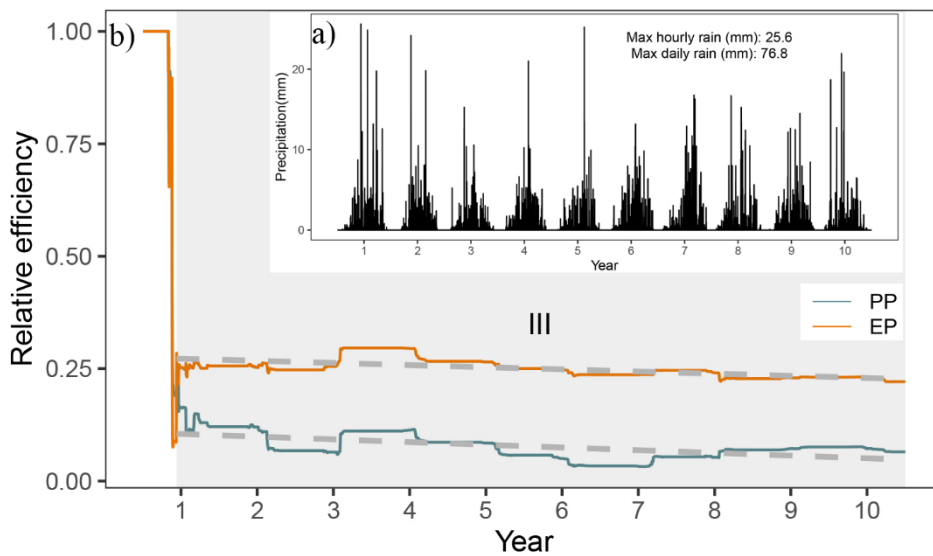
Figure 11: (a) rainfall downscaled from stochastic future rainfall; (b) the relative efficiency changes over ten years (grey region highlighting stage III, and the grey dashed lines indicated the linear fitting curve)

6. Conclusions

In this study, we compared the scenarios intervened by check dams, biological measures and artificial barriers using the C-L model to outline the affected area, measure the impacts of blocking sediment, and examine how the vegetable revetments helped to stabilise the slope. We have four key findings. First, the engineering works in controlling sediment transport are efficient, and it would be better at protecting the fragile environment effectively with other intervention measures like vegetation revetment and artificial barries. Second, the effectiveness of conservation and mitigation would decrease over time. Third, the characteristics of sediment transport patterns changed considerably by the intervention measures. The stabilising sediment ability in the source area increased by 161.9% with the additional help of vegetation revetments. At last, the present intervention measures are inadequate to reduce erosion and should be combined with dredging work.

Declaration of interest statement

The authors declare that they have no known competing financial interests or personal relationships that could have appeared to influence the work reported in this paper.

Author contribution

Di Wang: Conceptualisation, Methodology, Software, Writing-original draft preparation. Ming Wang and Kai Liu: Supervision, Methodology, Writing- Reviewing and Editing, Validation.

426   **Reference**

427   Bates, P. D., Horritt, M. S., and Fewtrell, T. J.: A simple inertial formulation of the shallow water equations for efficient

428   two-dimensional flood inundation modelling, J. Hydrol., 387, 33–45, https://doi.org/10.1016/j.jhydrol.2010.03.027, 2010.

429   Batty, M. and Xie, Y.: Possible urban automata, Environ. Plan. B Plan. Des., 24, 175–192, https://doi.org/10.1068/b240175,

430   1997.

431   Beven, K.: Linking parameters across scales: subgrid parameterizations and scale dependent hydrological models, Hydrol.

432   Process., 9, 507–525, https://doi.org/https://doi.org/10.1002/hyp.3360090504, 1995.

433   Beven, K.: TOPMODEL:A critical, Hydrol. Process., 11, 1069–1085, https://doi.org/https://doi.org/10.1002/(SICI)1099-

434   1085(199707)11:9<1069::AID-HYP545>3.0.CO;2-O, 1997.

435   Beven, K. J. and Kirkby, M. J.: A physically based, variable contributing area model of basin hydrology, Hydrol. Sci. Bull.,

436   24, 43–69, https://doi.org/10.1080/02626667909491834, 1979.

437   Chen, N., Zhou, H., Yang, L., Yang, L., and Lv, L.: Analysis of benefits of debris flow control projects in southwest

438   mountains areas of China, J. Chengdu Univ. Technol. (Science Technol. Ed., 40, 50–58, https://doi.org/10.3969/j.issn.1671-

439   9727.2013.01.008, 2013.

440   Chen, X., Li, Z., Cui, P., and Liu, X.: Estimation of soil erosion caused by the 5.12 Wenchuan Earthquake, J. Mt. Sci., 27,

441   122–127, 2009.

442   Cong, K., Li, R., and Bi, Y.: Benefit evaluation of debris flow control engineering based on the FLO-2D model, Northwest.

443   Geol., 52, https://doi.org/10.19751/j.cnki.61-1149/p.2019.03.019, 2019.

444   Couclelis, H.: From cellular automata to urban models: new principles for model development and implementation, Environ.

445   Plan. B Plan. Des., 24, 165–174, https://doi.org/10.1068/b240165, 1997.

446   Coulthard, T. J. and Skinner, C. J.: The sensitivity of landscape evolution models to spatial and temporal rainfall resolution,

447   Earth Surf. Dyn., 4, 757–771, https://doi.org/10.5194/esurf-4-757-2016, 2016.

448   Coulthard, T. J. and Van De Wiel, M. J.: Modelling long term basin scale sediment connectivity, driven by spatial land use

449   changes, Geomorphology, 277, 265–281, https://doi.org/10.1016/j.geomorph.2016.05.027, 2017.

450   Coulthard, T. J., Macklin, M. G., and Kirkby, M. J.: A cellular model of Holocene upland river basin and alluvial fan

451   evolution, Earth Surf. Process. Landforms, 27, 269–288, https://doi.org/10.1002/esp.318, 2002.

452   Coulthard, T. J., Hancock, G. R., and Lowry, J. B. C.: Modelling soil erosion with a downscaled landscape evolution model,

453   Earth Surf. Process. Landforms, 37, 1046–1055, https://doi.org/10.1002/esp.3226, 2012a.

454   Coulthard, T. J., Ramirez, J., Fowler, H. J., and Glenis, V.: Using the UKCP09 probabilistic scenarios to model the amplified

455   impact of climate change on drainage basin sediment yield, Hydrol. Earth Syst. Sci., 16, 4401–4416,

456   https://doi.org/10.5194/hess-16-4401-2012, 2012b.

457   Coulthard, T. J., Neal, J. C., Bates, P. D., Ramirez, J., de Almeida, G. A. M., and Hancock, G. R.: Integrating the

458   LISFLOOD-FP 2D hydrodynamic model with the CAESAR model: Implications for modelling landscape evolution, Earth

459   Surf. Process. Landforms, 38, 1897–1906, https://doi.org/10.1002/esp.3478, 2013.

460   Cui, P. and Lin, Y.: Debris-Flow Treatment: The Integration of Botanical and Geotechnical Methods, J. Resour. Ecol., 4,

461   097–104, https://doi.org/10.5814/j.issn.1674-764x.2013.02.001, 2013.

462   Cui, P., Zhou, G. G. D., Zhu, X. H., and Zhang, J. Q.: Scale amplification of natural debris flows caused by cascading

463   landslide dam failures, Geomorphology, 182, 173–189, https://doi.org/10.1016/j.geomorph.2012.11.009, 2013.

464   East, A. E. and Sankey, J. B.: Geomorphic and Sedimentary Effects of Modern Climate Change: Current and Anticipated

465   Future Conditions in the Western United States, Rev. Geophys., 58, https://doi.org/10.1029/2019RG000692, 2020.

466   Einstein, H. A.: The Bed-Load Function for Sediment Transportation in Open Channel Flows, 1950.

467   Fan, X., Yang, F., Siva Subramanian, S., Xu, Q., Feng, Z., Mavrouli, O., Peng, M., Ouyang, C., Jansen, J. D., and Huang, R.:

468   Prediction of a multi-hazard chain by an integrated numerical simulation approach: the Baige landslide, Jinsha River, China,

469   Landslides, 17, 147–164, https://doi.org/10.1007/s10346-019-01313-5, 2020.

470   Feng, W., He, S., Liu, Z., Yi, X., and Bai, H.: Features of Debris Flows and Their Engineering Control Effects at Xinping

471   Gully of Pingwu County, J. Eng. Geol., 25, https://doi.org/10．13544／j．cnki．jeg．2017．03．027, 2017.

472   Forbes, K. and Broadhead, J.: Forests and landslides: the role of trees and forests in the prevention of landslides and

473   rehabilitation of landslide-affected areas in Asia, FAO, 14–18 pp., 2013.

474   Gioia, D. and Schiattarella, M.: Modeling Short-Term Landscape Modification and Sedimentary Budget Induced by Dam

475   Removal: Insights from LEM Application, Appl. Sci., 10, 7697, https://doi.org/10.3390/app10217697, 2020.

476   Goldberg, D. E.: Genetic Algorithms in Search, Optimization, and Machine Learning, Addison-Wesley Longman Publishing

477   Co., Inc., 372 pp., https://doi.org/10.1007/BF01920603, 1989.

478   Gorum, T., Fan, X., van Westen, C. J., Huang, R. Q., Xu, Q., Tang, C., and Wang, G.: Distribution pattern of earthquake-

479   induced landslides triggered by the 12 May 2008 Wenchuan earthquake, Geomorphology, 133, 152–167,

480   https://doi.org/10.1016/j.geomorph.2010.12.030, 2011.

481   Guo, Q., Xiao, J., and Guan, X.: The characteristics of debris flow activities and its optimal timing for the control in Shikan

482   River Basin Pingwu Country, Chinese J. Geol. Hazard Control, 29, https://doi.org/10. 16031/j. cnki. issn. 1003-8035. 2018.

483   03. 05, 2018.

484   Hancock, G. R., Verdon-Kidd, D., and Lowry, J. B. C.: Soil erosion predictions from a landscape evolution model – An

485   assessment of a post-mining landform using spatial climate change analogues, Sci. Total Environ., 601–602, 109–121,

486   https://doi.org/10.1016/j.scitotenv.2017.04.038, 2017.

487   Hassanli, A. M. and Beecham, S.: Criteria for optimizing check dam location and maintenance requirements, Check Dams,

488   Morphol. Adjust. Eros. Control Torrential Streams, 11–31, 2013.

489   He, J., Zhang, L., Fan, R., Zhou, S., Luo, H., and Peng, D.: Evaluating effectiveness of mitigation measures for large debris

490   flows in Wenchuan, China, Landslides, 19, 913–928, https://doi.org/10.1007/s10346-021-01809-z, 2022.

491   Huang, R.: Geohazard assessment of the Wenchuan earthquake, Science Press, Beijing, 944 pp., 2009.

492   Huang, R. and Fan, X.: The landslide story, Nat. Geosci., 6, 325–326, https://doi.org/10.1038/ngeo1806, 2013.

493   J.B.C.Lowry, M.Narayan, G.R.Hancock, K.G.Evans, and K.G.Evans: Understanding post-mining landforms:Utilising pre-

494   mine geomorphology to improve rehabilitation outcomes, Geomorphology, 328, 93–107,

495   https://doi.org/10.1016/j.geomorph.2018.11.027, 2019.

496   Lan, H., Wang, D., He, S., Fang, Y., Chen, W., Zhao, P., and Qi, Y.: Experimental study on the effects of tree planting on

497   slope stability, Landslides, 17, 1021–1035, https://doi.org/10.1007/s10346-020-01348-z, 2020.

498   Lee, T. and Jeong, C.: Nonparametric statistical temporal downscaling of daily precipitation to hourly precipitation and

499   implications for climate change scenarios, J. Hydrol., 510, 182–196, https://doi.org/10.1016/j.jhydrol.2013.12.027, 2014.

500   Li, C., Wang, M., and Liu, K.: A decadal evolution of landslides and debris flows after the Wenchuan earthquake,

501   Geomorphology, 323, 1–12, https://doi.org/10.1016/j.geomorph.2018.09.010, 2018.

502   Li, C., Wang, M., Liu, K., and Coulthard, T. J.: Landscape evolution of the Wenchuan earthquake-stricken area in response

503   to future climate change, J. Hydrol., 590, 125244, https://doi.org/10.1016/j.jhydrol.2020.125244, 2020.

504   Luan, J., Miao, P., Tian, X., Li, X., Ma, N., Xu, Z., Wang, H., and Zhang, Y.: Separating the impact of check dams on runoff

505   from climate and vegetation changes, J. Hydrol., 614, 128565, https://doi.org/10.1016/j.jhydrol.2022.128565, 2022.

506   Marchi, L., Comiti, F., Crema, S., and Cavalli, M.: Channel control works and sediment connectivity in the European Alps,

507   Sci. Total Environ., 668, 389–399, https://doi.org/10.1016/j.scitotenv.2019.02.416, 2019.

Mickovski, S. B., Bengough, A. G., Bransby, M. F., Davies, M. C. R., Hallett, P. D., and Sonnenberg, R.: Material stiffness, branching pattern and soil matric potential affect the pullout resistance of model root systems, Eur. J. Soil Sci., 58, 1471–1481, https://doi.org/10.1111/j.1365-2389.2007.00953.x, 2007.

Poeppl, R. E., Coulthard, T., Keesstra, S. D., and Keiler, M.: Modeling the impact of dam removal on channel evolution and sediment delivery in a multiple dam setting, Int. J. Sediment Res., 34, 537–549, https://doi.org/10.1016/j.ijsrc.2019.06.001, 2019.

Ramirez, J. A., Zischg, A. P., Schürmann, S., Zimmermann, M., Weingartner, R., Coulthard, T., and Keiler, M.: Modeling the geomorphic response to early river engineering works using CAESAR-Lisflood, Anthropocene, 32, https://doi.org/10.1016/j.ancene.2020.100266, 2020.

Ramirez, J. A., Mertin, M., Peleg, N., Horton, P., Skinner, C., Zimmermann, M., and Keiler, M.: Modelling the long-term geomorphic response to check dam failures in an alpine channel with CAESAR-Lisflood, Int. J. Sediment Res., 37, 687–700, https://doi.org/10.1016/j.ijsrc.2022.04.005, 2022.

Reichenbach, P., Busca, C., Mondini, A. C., and Rossi, M.: The Influence of Land Use Change on Landslide Susceptibility Zonation: The Briga Catchment Test Site (Messina, Italy), Environ. Manage., 54, 1372–1384, https://doi.org/10.1007/s00267-014-0357-0, 2014.

Saynor, M. J., Lowry, J. B. C., and Boyden, J. M.: Assessment of rip lines using CAESAR-Lisflood on a trial landform at the Ranger Uranium Mine, L. Degrad. Dev., 30, 504–514, https://doi.org/10.1002/ldr.3242, 2019.

Skinner, C. J., Coulthard, T. J., Schwanghart, W., Van De Wiel, M. J., and Hancock, G.: Global sensitivity analysis of parameter uncertainty in landscape evolution models, Geosci. Model Dev., 11, 4873–4888, https://doi.org/10.5194/gmd-11-4873-2018, 2018.

Slingerland, N., Beier, N., and Wilson, G.: Stress testing geomorphic and traditional tailings dam designs for closure using a landscape evolution model, in: Proceedings of the 13th International Conference on Mine Closure, 1533–1544, https://doi.org/10.36487/ACG_rep/1915_120_Slingerland, 2019.

Stokes, A., Douglas, G. B., Fourcaud, T., Giadrossich, F., Gillies, C., Hubble, T., Kim, J. H., Loades, K. W., Mao, Z., McIvor, I. R., Mickovski, S. B., Mitchell, S., Osman, N., Phillips, C., Poesen, J., Polster, D., Preti, F., Raymond, P., Rey, F., Schwarz, M., and Walker, L. R.: Ecological mitigation of hillslope instability: Ten key issues facing researchers and practitioners, Plant Soil, 377, 1–23, https://doi.org/10.1007/s11104-014-2044-6, 2014.

Thomson, H. and Chandler, L.: Tailings storage facility landform evolution modelling, in: Proceedings of the 13th International Conference on Mine Closure, 385–396, https://doi.org/10.36487/ACG_rep/1915_31_Thomson, 2019.

Wang, M., Yang, W., Shi, P., Xu, C., and Liu, L.: Diagnosis of vegetation recovery in mountainous regions after the wenchuan earthquake, IEEE J. Sel. Top. Appl. Earth Obs. Remote Sens., 7, 3029–3037, https://doi.org/10.1109/JSTARS.2014.2327794, 2014a.

Wang, M., Liu, M., Yang, S., and Shi, P.: Incorporating Triggering and Environmental Factors in the Analysis of Earthquake-Induced Landslide Hazards, Int. J. Disaster Risk Sci., 5, 125–135, https://doi.org/10.1007/s13753-014-0020-7, 2014b.

Wang, N., Han, B., Pang, Q., and Yu, Z.: post-evaluation model on effectiveness of debris flow control, J. Eng. Geol., 23, 219–226, https://doi.org/10.13544/j.cnki.jeg.2015.02.005, 2015.

Van De Wiel, M. J., Coulthard, T. J., Macklin, M. G., and Lewin, J.: Embedding reach-scale fluvial dynamics within the CAESAR cellular automaton landscape evolution model, Geomorphology, 90, 283–301, https://doi.org/10.1016/j.geomorph.2006.10.024, 2007.

Wilcock, P. R., Asce, M., and Crowe, J. C.: Surface-based Transport Model for Mixed-Size Sediment Surface-based Transport Model for Mixed-Size Sediment, 9429, https://doi.org/10.1061/(ASCE)0733-9429(2003)129, 2003.

Xie, J., Wang, M., Liu, K., and Coulthard, T. J.: Modeling sediment movement and channel response to rainfall variability after a major earthquake, Geomorphology, 320, 18–32, https://doi.org/10.1016/j.geomorph.2018.07.022, 2018.

Xu, C., Xu, X., Yao, X., and Dai, F.: Three (nearly) complete inventories of landslides triggered by the May 12, 2008 Wenchuan Mw 7.9 earthquake of China and their spatial distribution statistical analysis, Landslides, 11, 441–461, https://doi.org/10.1007/s10346-013-0404-6, 2014.

Yang, Z., Duan, X., Huang, J., Dong, Y., Zhang, X., Liu, J., and Yang, C.: Tracking long-term cascade check dam siltation: implications for debris flow control and landslide stability, Landslides, 18, 3923–3935, https://doi.org/10.1007/s10346-021-01755-w, 2021.

Yeh, A. G. O. and Li, X.: Errors and uncertainties in urban cellular automata, Comput. Environ. Urban Syst., 30, 10–28, https://doi.org/10.1016/j.compenvurbsys.2004.05.007, 2006.

Yu, B., Yang, Y., Su, Y., Huang, W., and Wang, G.: Research on the giant debris flow hazards in Zhouqu County, Gansu Province on August 7, 2010, J. Eng. Geol., 18, 437–444, https://doi.org/10.3969/j.issn.1004-9665.2010.04.001, 2010.

Zhang, L. and Liang, K.: Research on economic benefit evaluation of the prevention and cure project for debris flow, Chinese J. Geol. Hazard Control, 16, 48–53, https://doi.org/10.3969/j.issn.1003-8035.2005.03.011, 2005.

Zhang, X., Wang, M., Liu, K., Xie, J., and Xu, H.: Using NDVI time series to diagnose vegetation recovery after major earthquake based on dynamic time warping and lower bound distance, Ecol. Indic., 94, 52–61, https://doi.org/10.1016/j.ecolind.2018.06.026, 2018.

Zhou, H., Chen, N., Lu, Y., and Li, B.: Control Effectiveness of Check Dams in Debris Flow Gully: A Case of Huashiban Gully in Earthquake Worst-stricken Area，Beichuan County, J. Mt. Sci., 30, 347–354, https://doi.org/10.3969/j.issn.1008-2786.2012.03.015, 2012.